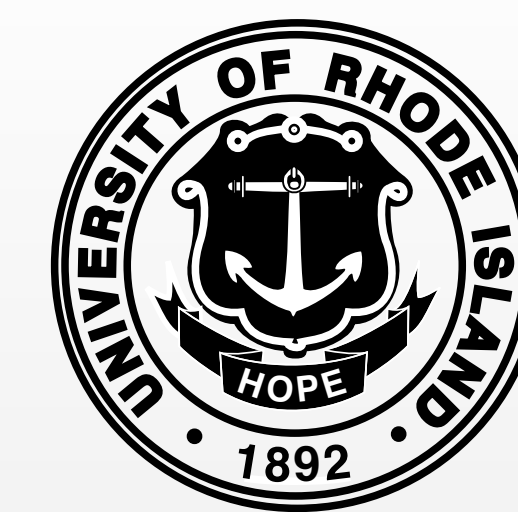




Adjoint tomography of the Middle East

DANIEL PETER¹ (dpeter@princeton.edu), BRIAN SAVAGE², ARTHUR RODGERS³, JEROEN TROMP¹

¹ DEPARTMENT OF GEOSCIENCES, PRINCETON UNIVERSITY, ² DEPARTMENT OF GEOSCIENCES, UNIVERSITY OF RHODE ISLAND, ³ LAWRENCE LIVERMORE NATIONAL LABORATORY, LIVERMORE, USA



Abstract (S53B-1977)

Improvements in **nuclear explosion monitoring** require refined seismic models of the target region. In our study, we focus on the Middle East, spanning a region from Turkey to the west and West India to the east. This area represents a complex geologic and tectonic setting with sparse seismic data coverage. This has led to diverging interpretations of crustal and underlying upper-mantle structure by different research groups, complicating seismic monitoring of the Middle East at regional distances. We evaluated an initial 3D seismic model of this region by computing full waveforms for several regional earthquakes by a spectral-element method. We measure **traveltimes and multitaper phase shifts** between observed broadband data and synthetic seismograms for distinct seismic phases within selected time windows using a recently developed **automated measurement algorithm**. Based on the remaining misfits, we setup an iterative inversion procedure for a fully numerical 3D seismic tomography approach. In order to improve the initial 3D seismic model, the **sensitivity to seismic structure** of the traveltime and multitaper phase measurements for all available seismic network recordings is computed. As this represents a computationally very intensive task, we take advantage of a fully numerical **adjoint approach** by using the efficient software package SPECFEM3D_GLOBE on a dedicated cluster. We show examples of such sensitivity kernels for different seismic events and use them in a **steepest descent approach** to update the 3D seismic model, starting at longer periods between 60 s and up to 200 s and moving towards shorter periods of 11 s. We highlight various improvements in the initial seismic structure during the iterations in order to better fit regional seismic waveforms in the Middle East.

Model and CMT Source Inversions

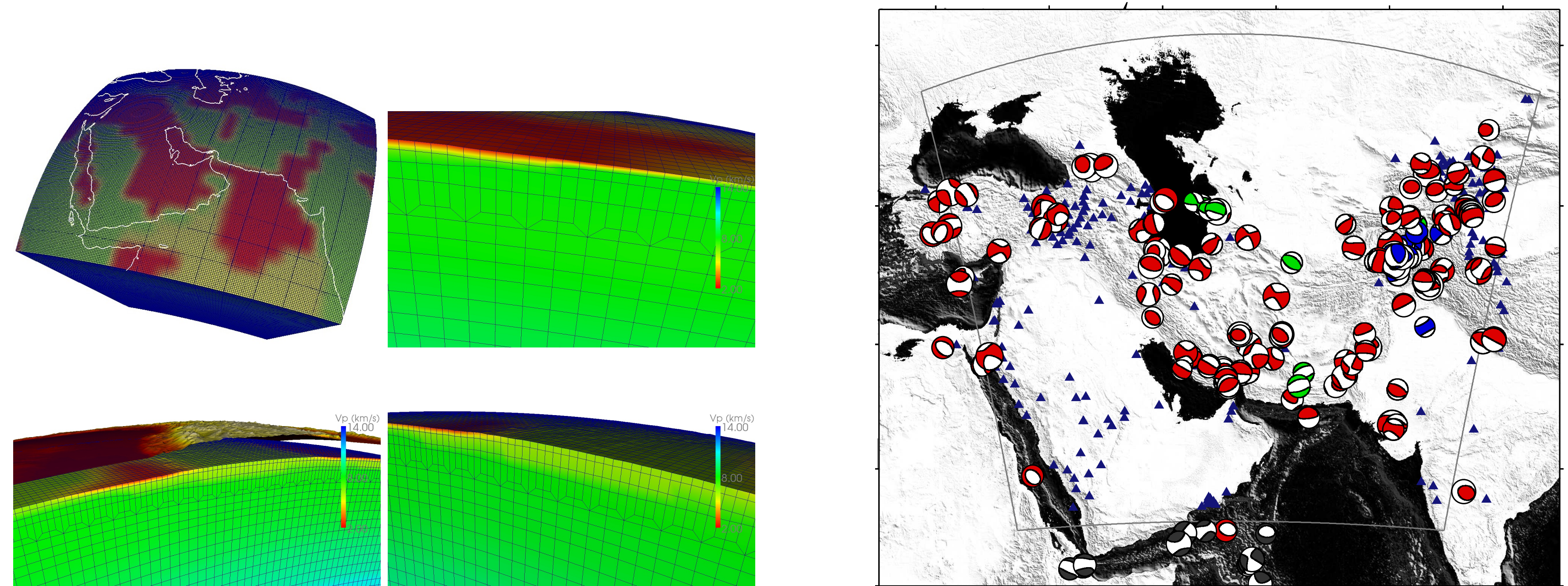


Fig. 1 Starting model S2.9EA (Kustowski et al., 2008) as implemented in SPECFEM3D_GLOBE (www.geodynamics.org). The mesh honors the Moho boundary for thin oceanic crust and thicker continental crust. This leads to a better crustal sampling and more accurate surface wave propagation with the spectral-element method.

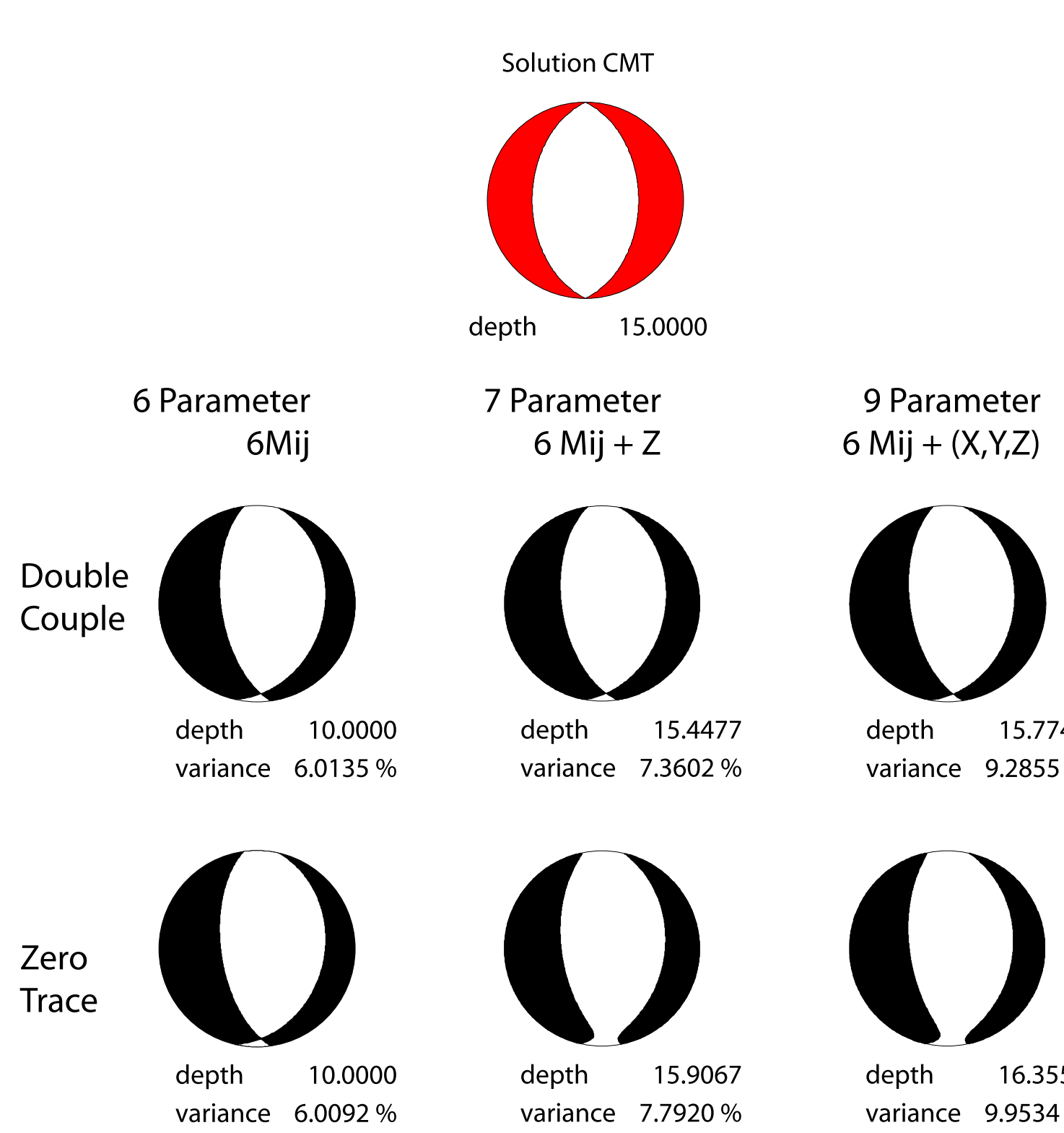


Fig. 2 Moment tensor solutions for 197 events in the region. Solutions are 7 parameter zero-trace, including the depth. Most solutions do not change appreciably when the number of parameters are changed or double couple constraints are imposed. Further, the solutions agree well with those published by globalcmt.org, in terms of the fault plane solution and the source depth.

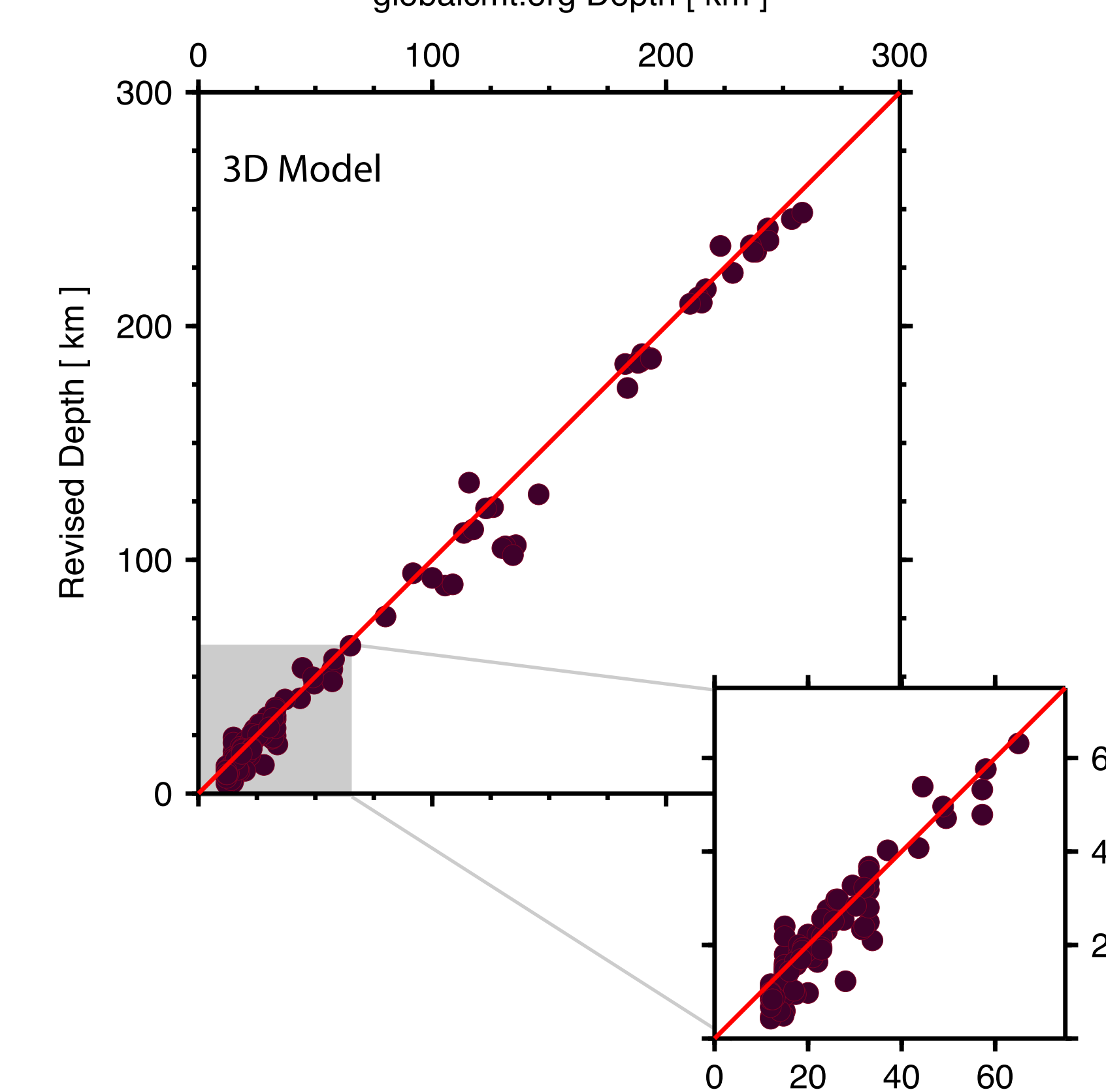


Fig. 3 Performance of the CMT Inversion (Liu et al. 2004) to recover faulting parameters and source depth from a synthetic event (red, top) using several different parameterizations (black). Variance reductions and optimal depth for each parameterization are displayed beneath each moment tensor. Synthetics were computed using the S2.9EA wave speed model of the region and initial solution depth and moment tensor elements were different to force the inversion to recover the optimal solution (red). Zero trace, 7 parameter solutions are used as sources in the subsequent adjoint inversions.

Adjoint kernels

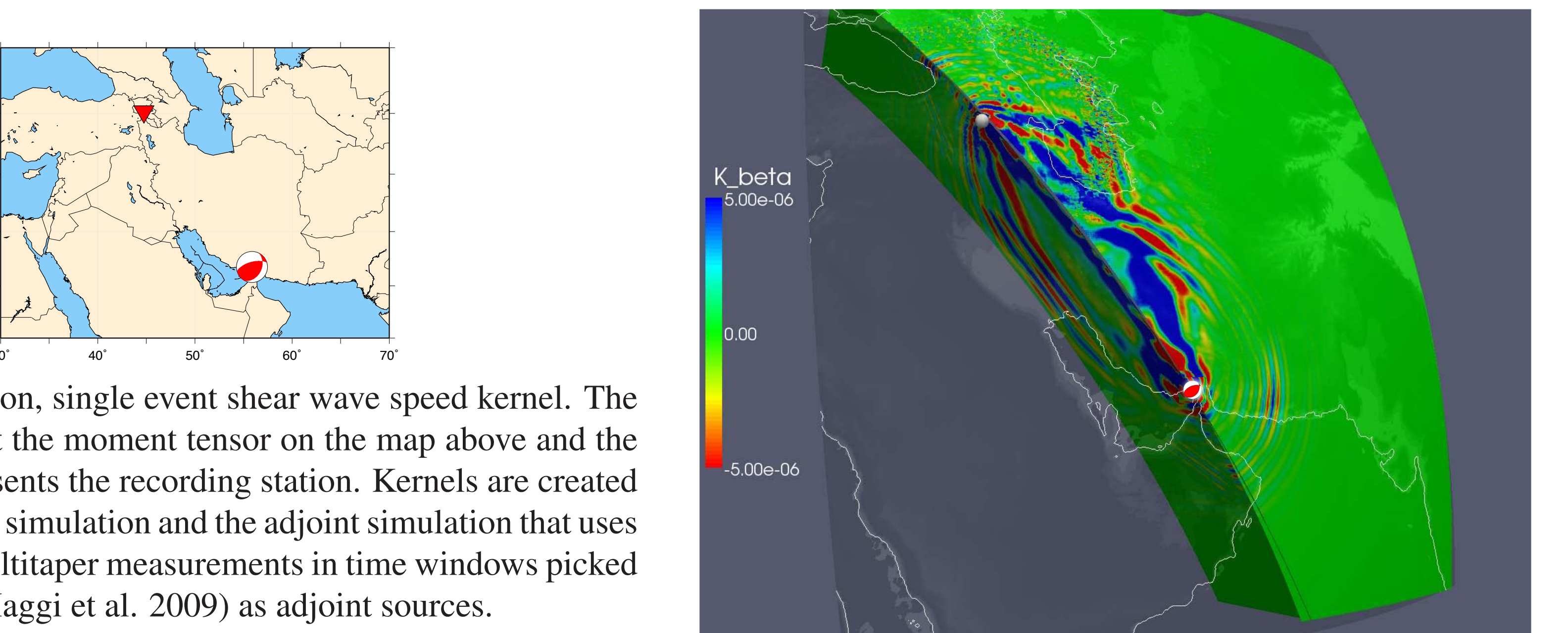


Fig. 5 Single station, single event shear wave speed kernel. The event is located at the moment tensor on the map above and the red triangle represents the recording station. Kernels are created through a forward simulation and the adjoint simulation that uses traveltimes and multitaper measurements in time windows picked by FLEXWIN (Maggi et al. 2009) as adjoint sources.

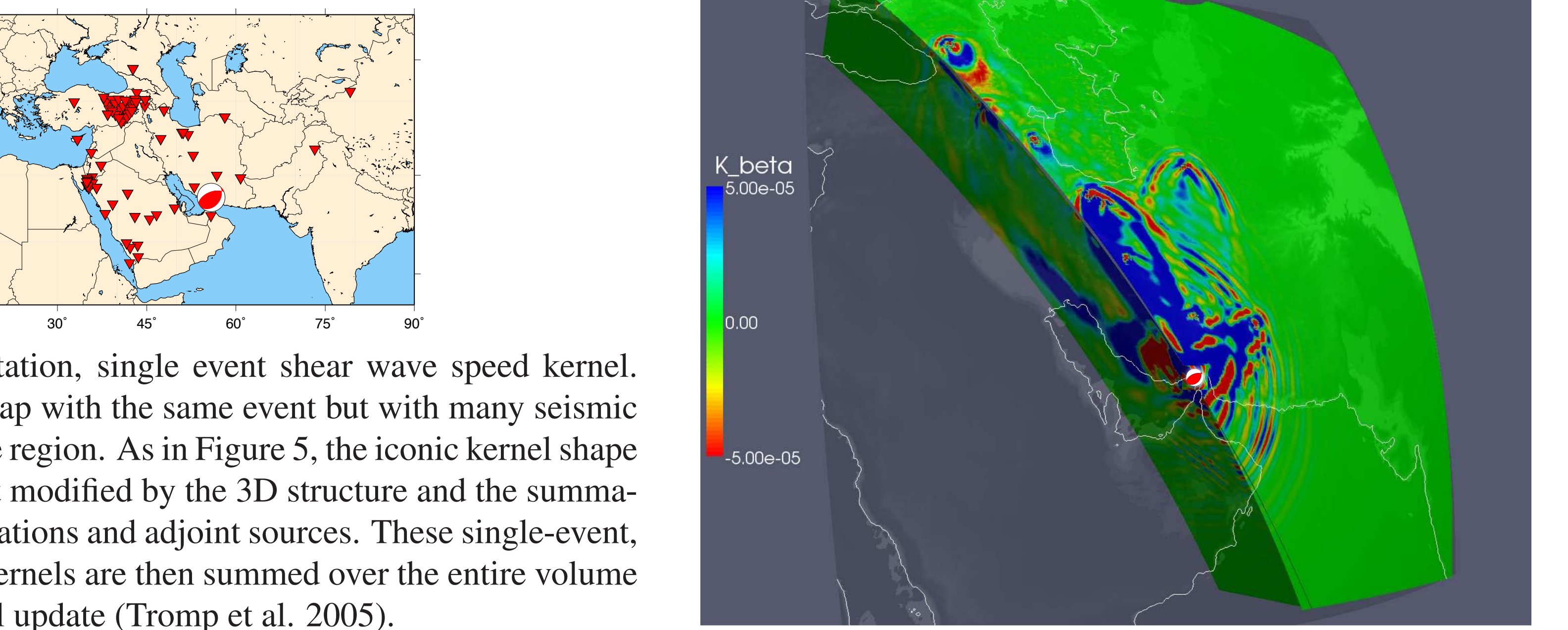


Fig. 6 Multiple station, single event shear wave speed kernel. Above shows a map with the same event but with many seismic stations within the region. As in Figure 5, the iconic kernel shape is identifiable, but modified by the 3D structure and the summation of multiple stations and adjoint sources. These single-event, multiple station kernels are then summed over the entire volume to build the model update (Tromp et al. 2005).

Adjoint tomography

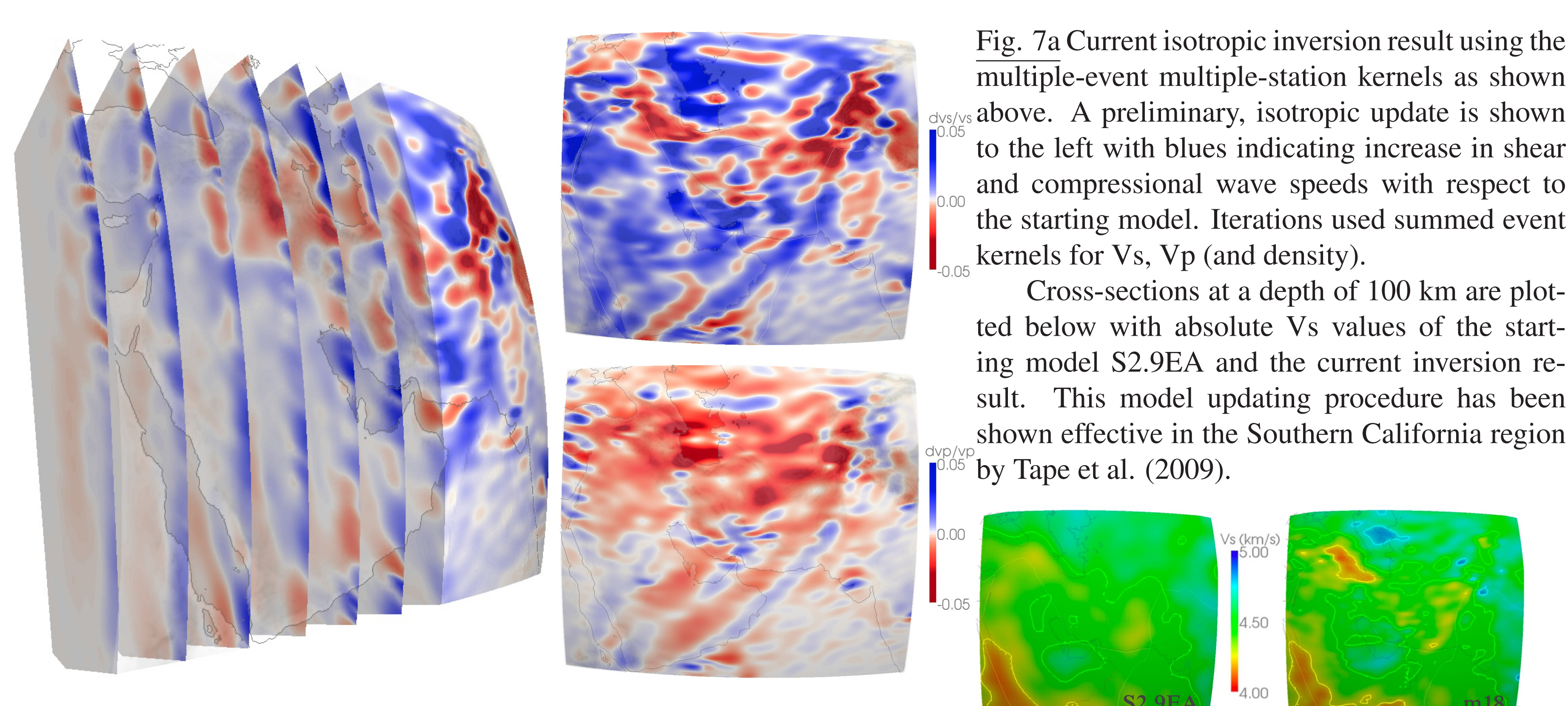
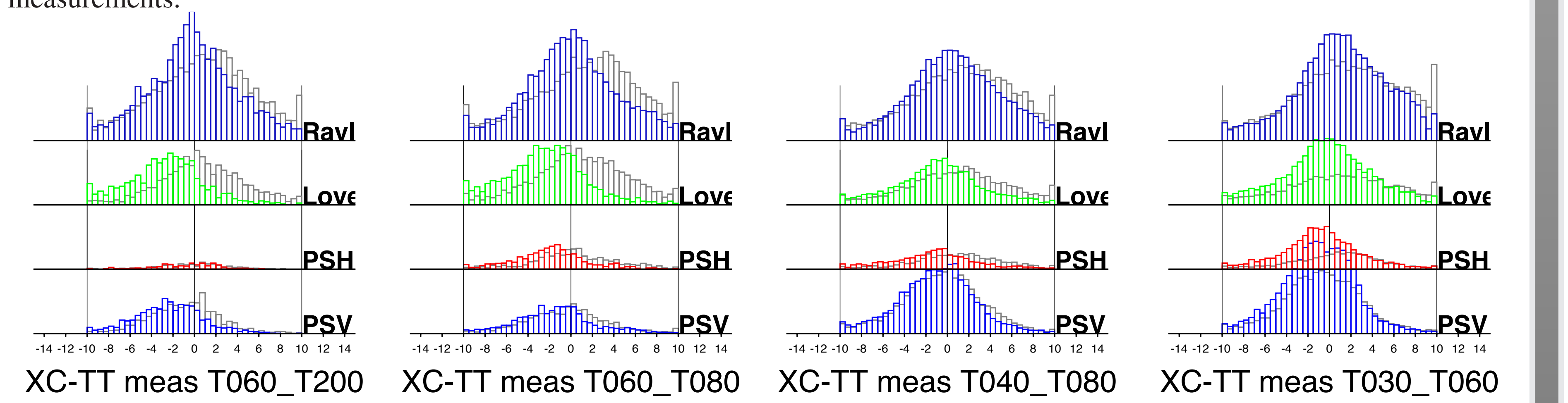


Fig. 7a Current isotropic inversion result using the multiple-event multiple-station kernels as shown above. A preliminary, isotropic update is shown to the left with blues indicating increase in shear and compressional wave speeds with respect to the starting model. Iterations used summed event kernels for Vs, Vp (and density).

Cross-sections at a depth of 100 km are plotted below with absolute Vs values of the starting model S2.9EA and the current inversion result. This model updating procedure has been shown effective in the Southern California region by Tape et al. (2009).

Fig. 7b Cross-correlation traveltime misfits for current inversion result (shown in color bars) and starting model (gray). Misfits are measured in four different period bands (60-200 s, 60-80 s, 40-80 s and 30-60 s) and separated in surface and body wave measurements.



Isotropic iterations

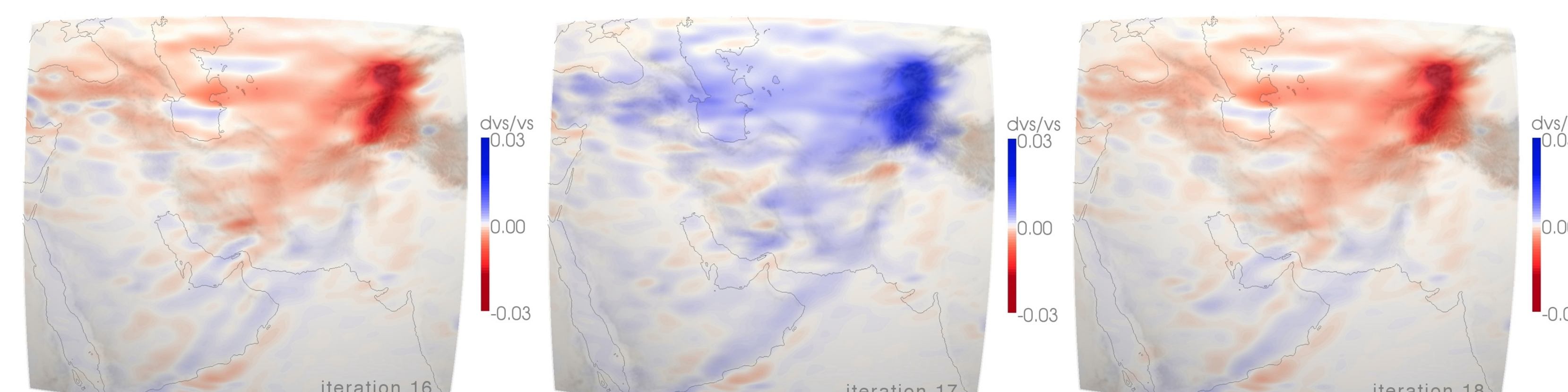


Fig. 8 Isotropic iterations show oscillations between successive model updates. These iterations are due to radial anisotropy in the upper mantle. Updated models switch between better fitting Rayleigh- or Love waves. This becomes especially pronounced for surface waves at 40 s and longer. Including long-period surface wave measurements in isotropic inversions will inhibit the model updates to converge. Small-scale structural perturbations are dominated by these Rayleigh/Love wave discrepancies.

Radial anisotropic updates

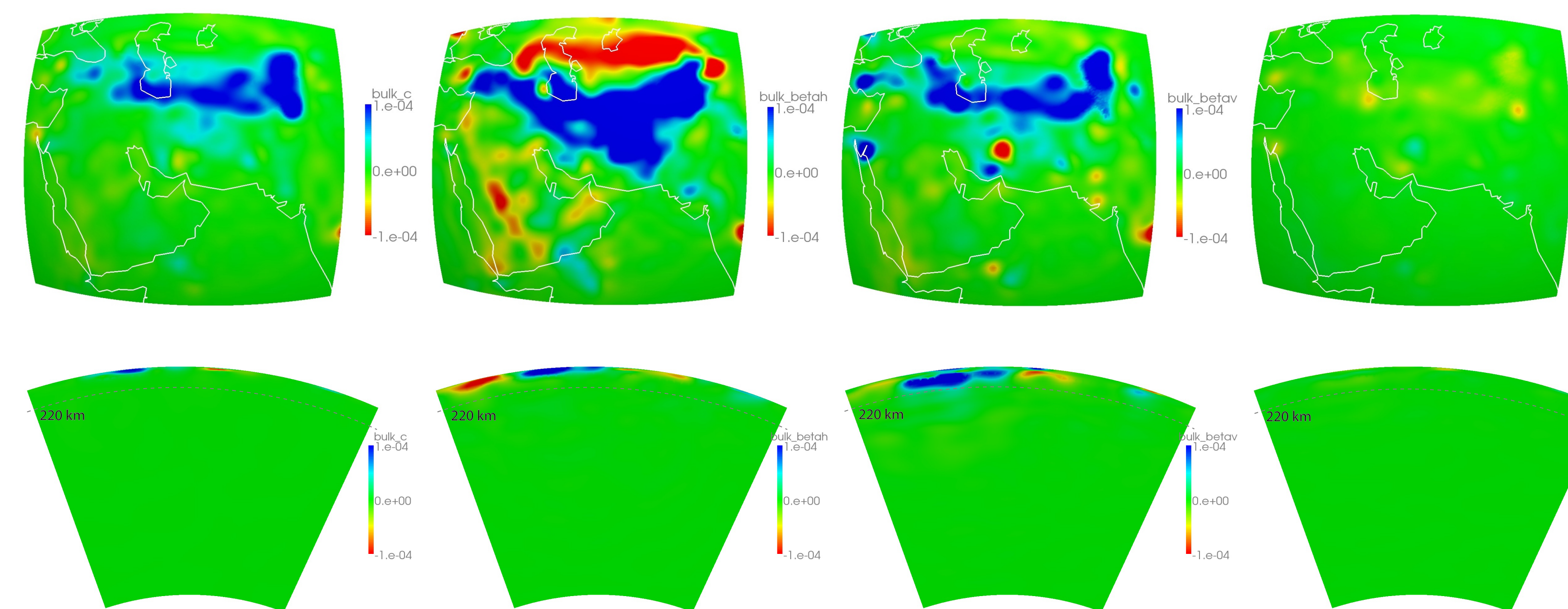


Fig. 9 Anisotropic model update taking account of radial anisotropy in the upper mantle. The gradients have been smoothed horizontally/vertically with a 3D Gaussian filter. Regional scale inversions have to include radial anisotropic model updates. A suitable set of adjoint kernels becomes:

$$\text{bulk : } K_{\Phi} = \frac{\Phi^2}{\alpha_h^2} K_{\alpha_h} + \frac{\Phi^2}{\alpha_v^2} K_{\alpha_v} \quad (1)$$

$$\text{eta : } K_{\eta} = F K_F \quad (2)$$

$$\text{horizontal shear : } K'_{\beta_h} = K_{\beta_h} + \frac{4}{3} \frac{\beta_h^2}{\alpha_h^2} K_{\alpha_h} \quad (3)$$

$$\text{vertical shear : } K'_{\beta_v} = K_{\beta_v} + \frac{4}{3} \frac{\beta_v^2}{\alpha_v^2} K_{\alpha_v} \quad (4)$$

where K_{α_h} , K_{α_v} , K_{β_h} , and K_F are the transverse isotropic kernel expressions from Sieminski et al. (2007). For radial anisotropic model updates, density ρ will be scaled to the isotropic shear wave kernel.

Conclusion

Isotropic model updates suffer from oscillations at longer periods (> 40 s), trying to fit Rayleigh and Love waves. Inverting for radial anisotropy will diminish this **surface wave discrepancy** and allow to fit data at shorter periods, thus leading to higher resolution in regional tomographic images.

Future plans involve calculating **radial anisotropic event kernels** to update anisotropic layers between Moho and 220 km depth of the Middle East region. The computation of sensitivity kernels for radial anisotropic parameters has been readily implemented in the SPECFEM3D_GLOBE package. The new model updates will also take advantage of a preconditioned **conjugate-gradient approach** for faster convergence.

References

- Komatitsch, D., and J. Tromp (1999), *Introduction to the spectral-element method for 3-D seismic wave propagation*, Geophys. J. Int., **139**, 806 - 822.
- Kustowski, B., G. Ekström, and A. M. Dziewonski (2008), *The shear-wave velocity structure in the upper mantle beneath eurasia*, Geophys. J. Int., **174**, 978 - 992, doi:10.1111/j.1365-246X.2008.03865.x.
- Liu, Q., J. Polet, D. Komatitsch, and J. Tromp (2004), *Spectral-Element Moment Tensor Inversions for Earthquakes in Southern California*, Bull. Seism. Soc. Am., **94**(5), 1748 - 1761, doi:10.1785/012004038.
- Maggi, A., C. Tape, M. Chen, D. Chao, and J. Tromp (2009), *An Automated time-window selection algorithm for seismic tomography*, Geophys. J. Int., **178**(1), 257 - 281, doi:10.1111/j.1365 - 246X.2009.04099.x.
- Sieminski, A., Q. Liu, J. Trampert, and J. Tromp (2007), *Finite-frequency sensitivity of body waves to anisotropy based upon adjoint methods*, Geophys. J. Int., **171**(1), 368 - 389.
- Tape, C., Q. Liu, A. Maggi, and J. Tromp (2009), *Adjoint tomography of the Southern California crust*, Science, **325**, 988 - 992.
- Tromp, J., C. Tape, and Q. Liu (2005), *Seismic tomography, adjoint methods, time reversal and banana-doughnut kernels*, Geophys. J. Int., **160**(1), 195 - 216.